



Diffusive terms applied in smoothed particle hydrodynamics simulations of incompressible and isothermal Newtonian fluid flows

Carlos Alberto Dutra Fraga Filho^{1,2,3} · Fábio Pavan Piccoli^{1,3}

Received: 31 January 2021 / Accepted: 11 August 2021 / Published online: 4 October 2021
© The Brazilian Society of Mechanical Sciences and Engineering 2021

Abstract

Currently, there is not an extensive literature dedicated to the presentation of the diffusive modeling applied to the momentum equation of incompressible and isothermal Newtonian fluid flows solved by the smoothed-particle hydrodynamics (SPH) method. This paper aims to present the most common viscosity modelings and the LES (Large Eddy Simulation) method applied to the solution of the Navier–Stokes (N–S) equations. A comparative study showing different modelings of the diffusive terms has been carried out. Two incompressible free surface flows were simulated: the generation and propagation of waves on a flat beach and the collapse of a water column. In the first case study, the SPH results were compared to the results provided by the Eulerian modeling (Boussinesq-type nonlinear wave equations solved by the finite difference method and validated from laboratory data). It was verified that the laminar shear stress modeling is the most adequate in the wave period and wave amplitude simulated, although great divergences have not been noticed in relation to the other models used. In the collapse of the water column study, the SPH results obtained after implementation of different approaches for the diffusive terms of the N–S equations presented good agreement with experimental or literature data.

Keywords SPH simulations · Turbulence · Large eddy simulation · SGS shear stresses · Artificial viscosity

List of symbols

a	Superscript that refers to the fixed particle	C_l	Constant in the sub-grid scale (SGS) shear stress tensor calculus
b	Superscript that refers to the neighbor particle	C_s	Smagorinsky constant
B	Coefficient related to the fluctuations of density	$\frac{d}{dt}$	Material or substantive derivative
c	Sound velocity in the fluid	\tilde{f}	Favre average of the function f
		\mathbf{g}	Gravity in vectorial notation
		g_i	Gravity in Einstein notation
		h	Smoothing length
		h	Mean sea level
		H	Total depth
		i	Subscript that refers to the Cartesian directions
		j	Subscript that refers to the Cartesian directions
		k	Scale factor that depends on the kernel employed in the interpolations
		kh	Support radius
		m	Mass
		n	Number of neighboring particles
		P	Pressure
		P_{dyn}^a	Dynamic pressure acting on the fixed particle
		\tilde{S}_{ij}	Strain rate tensor
		t	Time

Technical Editor: Daniel Onofre de Almeida Cruz.

✉ Carlos Alberto Dutra Fraga Filho
cadff1@gmail.com

¹ Federal Institute of Education, Science and Technology of Espírito Santo (IFES), Development, Implementation and Application of Computational Tools for Problem Solving in Engineering Research Group, Av. Vitória, 1729, Jucutuquara, Vitória, ES 29040-780, Brazil

² ESS Engineering Software Steyr GmbH, Berggasse 35, 4400 Steyr, Austria

³ Laboratory of Simulation of Free Surface Flows (LABESUL), Federal University of Espírito Santo (UFES), Postgraduate Programme in Environmental Engineering, Av. Fernando Ferrari, 514, Goiabeiras, Vitória, ES 29075-910, Brazil

u_j	Fluid velocity in Einstein notation
\mathbf{v}	Fluid velocity in vectorial notation
\mathbf{v}_{\max}	Maximum fluid velocity in the simulation
\mathbf{x}	Spatial position in vectorial notation
\mathbf{x}^a	Spatial position of the fixed particle
\mathbf{x}^b	Spatial position of the neighbor particle
x_i	Spatial position in Einstein notation
$ \mathbf{x} - \mathbf{x}' $	Distance between the position of a fixed and a variable point at the domain
$W(\mathbf{x} - \mathbf{x}', h)$	Smoothing function (kernel)
Greek symbols	
α_π	Coefficient used in the calculation of the artificial viscosity
γ	Exponent in the Tait equation
Δx	Initial particle spacing
δ_{ij}	Kronecker delta function
η	Surface elevation
k	Turbulence kinetic energy
μ	Dynamic fluid viscosity
ν	Kinematic fluid viscosity
ν^a	Kinematic viscosity of the fixed particle
ν_t	Eddy viscosity
Π_{ab}	Artificial viscosity
ρ	Fluid density
$\bar{\rho}$	Spatial filtered density
ρ^0	Density of the fluid in rest
τ^*	Sub-grid scale (SGS) shear stress tensor
τ_{ij}	Elements of the sub-grid scale (SGS) shear stress tensor
Ψ^a	Diffusive terms of the fixed particle related to the viscosity and turbulence effects
φ^2	Factor that prevents numerical differences when two particles approach one another
∇	Vector differential mathematical operator
$(\nu^a \nabla^2 \nu^a)_{\text{LAMINAR}}$	Laminar shear stresses of the fixed particle

1 Introduction

In principle, Navier–Stokes equations can be used to simulate both laminar and turbulent flows without averaging or approximations other than the necessary numerical discretizations [1]. Theoretically, with the employment of an

adequate numerical model, the conservation equations that describe physical phenomena involved in the sciences/ engineering problems could be solved.

There is the scarce literature dedicated to the study and implementation of approximations for the diffusive viscous terms and turbulence in the momentum equation (when solved using the incompressible SPH Lagrangian method). [2] is the recent and rare literature that deals with diffusive viscous terms in particle methods, which can be cited.

There are other references dedicated to the study of diffusive terms (numerical) in the SPH method, as [3–5], for example. The introduction of an additional diffusive term in the continuity equation (to reduce the numerical noise inside the density field obtained from the SPH interpolations) is proposed. Considering that the pressure field is evaluated from the density field, from a state equation, a smoother density field leads to a more accurate pressure field.

This paper is dedicated to the presentation of common modelings for the diffusive viscous terms in the momentum equation and turbulence used in particle simulations of incompressible and isothermal Newtonian fluid flows, with analysis of the results. Besides, a brief literature review on the turbulence models implemented in the momentum equation in SPH simulations is presented. Particular attention is given to the large eddy simulation (LES) turbulence model—utilized in this work with the application of the sub-grid scale (SGS) model.

In this work, four different approaches have been applied in the modeling of the diffusive terms in the momentum equation: (a) artificial viscosity, (b) laminar shear stress, (c) laminar shear stresses + turbulence model (LES) and (d) laminar shear stresses + artificial viscosity. Simulations have been performed for the generation and propagation of waves on a flat beach and the collapse of a water column.

In the first case studied, Lagrangian and Eulerian numerical models were applied in simulations. Numerical codes based on the Lagrangian SPH method (SPHysics) and Boussinesq-type nonlinear wave equations (FUNWAVE2D) were used. A detailed description of the SPHysics and FUNWAVE2D can be found in [6] and [7, 8], respectively.

In the collapse of a water column, two Lagrangian codes were used in the numerical simulations: SPHysics and the computational tool presented in [9, 10]. SPHysics code were validated for use in this specific problem from laboratory experiments [11, 12]. [13] brings some simulation results provided by SPHysics to this problem, using different viscosity treatments. The computational tool presented in [9, 10] employed a modeling of viscosity (laminar shear stresses + artificial viscosity) unavailable in SPHysics and validated from experimental data.

The remainder of this scientific work is organized as follows. In Sect. 2, the physical–mathematical modeling and the SPH method are presented. A brief literature review of turbulence models applied in SPH Method is provided to the reader in Sect. 3. Section 4 presents the viscosity and turbulence modelings employed in the simulations of this work. The numerical simulations performed and discussions are in Sect. 5. Finally, conclusions are presented in Sect. 6.

2 Physical–mathematical modeling

This section brings the physical–mathematical modeling used in this paper as well as a brief presentation of the smoothed-particle hydrodynamics method. A more complete presentation of the SPH method can be found in the literature [14].

2.1 Lagrangian particle modeling and the SPH method

The physical conservation equations (mass and momentum) employed in this paper to a Newtonian, incompressible and isothermal fluid flow are presented in Table 1 along with the respective SPH approximations.

The SPH method is employed in the solution of the partial differential equations used to express the physical conservation equations mathematically.

According to the Lagrangian approach, the continuum domain is discretized into a finite number of particles to obtain the physical properties from interpolations of the physical properties of the neighboring particles (inside a domain of influence with a support radius equal to kh). These interpolations employ smoothing functions (or kernels) that have to satisfy some properties: convergence, smoothness, positivity, symmetry, normalization within the support domain and compact support.

Figure 1 shows the disposition of the particles within the domain of influence. The fixed particle is located in the center of the local domain and its physical properties are obtained from the interpolation of the properties of the neighboring particles. The kernel guarantees the greatest

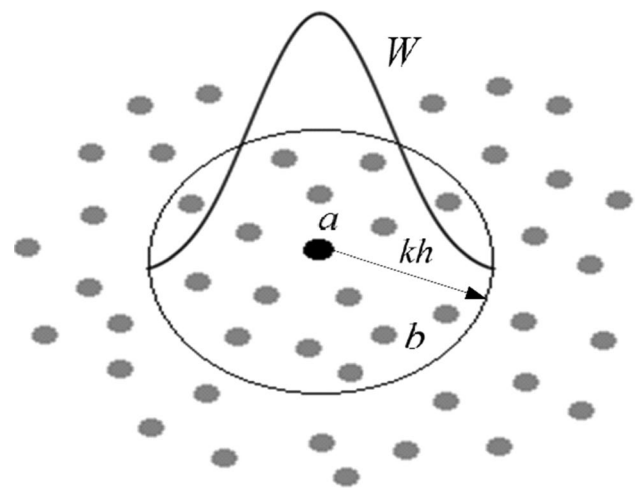


Fig. 1 Graphical representation of the domain of influence. The reference particle has as neighbors all particles within the domain defined by the circumference with support radius equal to kh

contribution of the nearest neighboring particles to the value of the physical quantity in the reference (fixed) particle.

Reprinted by permission from Springer: Springer Nature Switzerland AG. Smoothed Particle Hydrodynamics: Fundamentals and Basic Applications in Continuum Mechanics by Carlos Alberto Dutra Fraga Filho. Copyright 2019.

The cubic spline kernel, presented below, has been used in this work for 2-D simulations. Other kernels used in SPH interpolations could be found in [14].

$$W(\mathbf{x} - \mathbf{x}', h) = \frac{10}{7\pi h^2} \begin{cases} 1 - \frac{3}{2} \left(\frac{|\mathbf{x} - \mathbf{x}'|}{h}\right)^2 + \frac{3}{4} \left(\frac{|\mathbf{x} - \mathbf{x}'|}{h}\right)^3, & \text{if } 0 \leq |\mathbf{x} - \mathbf{x}'| \leq h \\ \frac{1}{4} \left(2 - \left(\frac{|\mathbf{x} - \mathbf{x}'|}{h}\right)^3\right), & \text{if } h < |\mathbf{x} - \mathbf{x}'| \leq kh \\ 0, & \text{in the other case.} \end{cases} \quad (3)$$

SPH provides approximations of the physical properties (such as density and temperature), gradients (such as the pressure gradients), divergences (such as the velocity divergences) and Laplacians (such as the Laplacian of

Table 1 Physical conservation equations and the SPH approximations

Partial differential equations (continuum domain)	SPH approximations (domain discretized by particles)
Continuity equation: $\frac{d\rho}{dt} = -\rho \nabla \cdot \mathbf{v}$	$\frac{d\rho^a}{dt} = \sum_{b=1}^n m^b (\mathbf{v}^a - \mathbf{v}^b) \cdot \nabla W(\mathbf{x}^a - \mathbf{x}^b, h)$ (1)
Momentum equation: $\frac{d\mathbf{v}}{dt} = -\frac{\nabla P}{\rho} + \nu \nabla^2 \mathbf{v} + \mathbf{g}$	$\frac{d\mathbf{v}^a}{dt} = -\sum_{b=1}^n m^b \left[\frac{P^a}{(\rho^a)^2} + \frac{P^b}{(\rho^b)^2} \right] \nabla W(\mathbf{x}^a - \mathbf{x}^b, h) + \Psi^a + \mathbf{g}$ (2)

temperature and Laplacian of velocities), with a second-order error [14].

In this method, in simulations for incompressible fluids, a state equation is used for the prediction of the pressure field. In this paper, the Tait equation was used:

$$P_{dyn}^a = B \left(\left(\frac{\rho^a}{\rho^0} \right)^\gamma - 1 \right) \quad (4)$$

$$B = \frac{c^2 \rho^0}{\gamma} \quad (5)$$

where $\gamma = 7$, for incompressible fluid simulations.

In order for the Tait equation to be applied in the prediction of the pressure field of the fluid, the maximum value of the Mach number must be 0.10. Thus, $c = 10 |\mathbf{v}_{\max}|$, where \mathbf{v}_{\max} is the maximum velocity of the fluid in the simulation.

The next section brings a brief explanation of turbulence concepts and especially of the LES turbulence model.

3 Brief literature review of turbulence models applied to the SPH method

Direct numerical simulation (DNS) is the first and most intuitive method employed in an attempt to capture the turbulence effects in fluid flows. The whole spectrum of turbulence scales from solving Navier–Stokes equations (no other modeling is required) is resolved. The discretization of the domain must capture all the dissipation of kinetic energy in the numerical solution of the conservation equations in a high number of spatial points defined in the domain (from the smallest dissipative scales—Kolmogorov microscales, up to the integral scale, associated with the motions containing most of the kinetic energy). DNS requires an extremely refined spatial and temporal discretization (with a great computational effort) leading to good results for low Reynolds numbers, which is a small fraction of the problems in the universe of fluid dynamics [14]. The literature presents successful applications of DNS in the particle simulation of decaying turbulence in a nonslip square box [15] and laminar periodic hill flow [16].

In most realistic turbulent flows, which present moderate to high Reynolds numbers, it is necessary to carry out the implementation of a turbulence model. The traditional closure turbulence models to the Reynolds-averaged Navier–Stokes (RANS) equations—using the Boussinesq eddy viscosity assumption, the mixing-length $\kappa - L_m$ model, the two-equation $\kappa - \varepsilon$ model and the explicit algebraic Reynolds stress (EARSMS) models—as well as the large eddy simulation (LES) model—are presented in [16], when applied to the smoothed-particle

hydrodynamics (SPH) method. Validation tests have been performed in the following cases: (a) open-channel turbulent steady flow ($\kappa - L_m$, $\kappa - \varepsilon$ and EARSMS), (b) 2-D collapse of a water column ($\kappa - L_m$, $\kappa - \varepsilon$ and EARSMS) (c) 3-D turbulent open-channel flow (LES) and (d) 3-D collapse of a water column (LES).

Large eddy simulation is a technique for turbulence modeling employed in various areas of fluid dynamics. Some important applications are presented in the literature: gas turbines [17]; atmospheric boundary layer [18]; wind tunnel simulations [19]; aeronautics, aeroacoustics and wall layer modeling [20, 21]; simulations of closed turbulent channel flow [22]; simulation of a near-shore solitary wave mechanics [23]; wave interaction with a floating breakwater [24]; breaking of plunging waves [25], among others.

LES is used in the simulation of large scales of turbulent motions. Using a spatial filter, LES divides turbulence flow into large-scale and small-scale (grid scale) motions. The large eddies contain most of the turbulent kinetic energy and are retained, and solved for directly from the averaged equations. The smaller scales of the turbulent motion extract and dissipate energy from the larger scales, and are removed from LES using a low-pass filter [6, 20, 21, 26–29]. As a consequence, in the resulting filtered equations, additional terms, called sub-grid scale (SGS) shear stresses, appear and will be solved by a closure turbulence model. When the grid size is sufficiently small, the impact from the sub-grid scale models on the flow motion will be small.

Favre-averaged filter is commonly used in the process of separation of the turbulence scales [6, 20, 26]. For a physical property f , the Favre-averaging is $\tilde{f} = \left(\overline{\rho f} \right) / \bar{\rho}$, where $-$ denotes a spatial filtering.

After passing the filter, the mass and momentum conservation equations for a Newtonian and incompressible fluid flow can be written (in Einstein notation) as follows:

$$\frac{\partial \bar{\rho}}{\partial t} + \frac{\partial (\bar{\rho} \tilde{u}_i)}{\partial x_i} = 0 \quad (6)$$

$$\frac{\partial (\bar{\rho} \tilde{u}_i)}{\partial t} + \frac{\partial (\bar{\rho} \tilde{u}_i \tilde{u}_j)}{\partial x_j} = - \frac{\partial \bar{P}}{\partial x_i} + \frac{\partial \left(2\mu \tilde{S}_{ij} - \frac{2}{3} \mu \delta_{ij} \tilde{S}_{ij} \right)}{\partial x_j} + \bar{\rho} g_i - \frac{\partial \tau^*}{\partial x_j} \quad (7)$$

where:

τ^* is the sub-grid scale (SGS) shear stress tensor which has the following elements:

$$\tau_{ij} = -\bar{\rho} (\tilde{u}_i \tilde{u}_j - \widetilde{u_i u_j}), (i, j) = 1, 2, 3 \quad (8)$$

$$\tilde{S}_{ij} = \frac{1}{2} \left(\frac{\partial \tilde{u}_i}{\partial x_j} + \frac{\partial \tilde{u}_j}{\partial x_i} \right), (i, j) = 1, 2, 3 \tag{9}$$

δ_{ij} is the Kronecker delta function ($\delta_{ij} = 1$, if $i = j$; $\delta_{ij} = 0$, if $i \neq j$) and $(i, j) = (1, 2, 3)$ represent the Cartesian directions.

To solve the LES equations using the SPH method, Eqs. (6)-(7) were written in the Lagrangian form:

$$\frac{d\bar{\rho}}{dt} = -\bar{\rho} \frac{\partial \tilde{u}_j}{\partial x_j} \tag{10}$$

$$\frac{d\tilde{u}_i}{dt} = -\frac{1}{\bar{\rho}} \frac{\partial \bar{P}}{\partial x_i} + \frac{1}{\bar{\rho}} \frac{\partial \left(2\mu \tilde{S}_{ij} - \frac{2}{3} \mu \delta_{ij} \tilde{S}_{ij} \right)}{\partial x_j} + g_i - \frac{1}{\bar{\rho}} \frac{\partial \tau^*}{\partial x_j} \tag{11}$$

The effects of the unresolved scales are contained in the SGS shear stress tensor and represent the motion that occurs on a scale smaller than the grid spacing Δx . In the SPH method, the SGS stress tensor represents the turbulent eddies smaller than the particle size [6]. There are different SGS models and most of them employ an eddy viscosity assumption (based on Boussinesq’s hypothesis) to model the shear stress tensor [21, 27, 29]. The formulation presented below for the components of the SGS stress tensor—according to [13]—was used in the simulations performed in this work:

$$\frac{\tau_{ij}}{\bar{\rho}} = \nu_t \left(2\tilde{S}_{ij} - \frac{2}{3} k \delta_{ij} \right) - \frac{2}{3} C_l \Delta^2 \delta_{ij} \left| \tilde{S}_{ij} \right|^2 \tag{12}$$

$$\left| \tilde{S}_{ij} \right| = \left\{ \begin{array}{l} 2 \left[\left(\frac{\partial \tilde{u}_1}{\partial x_1} \right)^2 + \left(\frac{\partial \tilde{u}_2}{\partial x_2} \right)^2 + \left(\frac{\partial \tilde{u}_3}{\partial x_3} \right)^2 \right] + \left(\frac{\partial \tilde{u}_1}{\partial x_2} + \frac{\partial \tilde{u}_2}{\partial x_1} \right)^2 \\ \left[\left(\frac{\partial \tilde{u}_1}{\partial x_3} + \frac{\partial \tilde{u}_3}{\partial x_1} \right)^2 + \left(\frac{\partial \tilde{u}_2}{\partial x_3} + \frac{\partial \tilde{u}_3}{\partial x_2} \right)^2 \right] \end{array} \right\}^{0.5} \tag{13}$$

where \tilde{S}_{ij} is the strain rate tensor, i and j are subindexes that refer to the Cartesian directions.

$$\Delta = \frac{(2\Delta x^2)^{0.5}}{2}$$

Eddy viscosity models are used to determine ν_t . Using the equilibrium assumption (that the turbulence in a grid with small-scale eddies is in equilibrium, and the dissipated energy is implemented from the large-scale eddies), the Smagorinsky model [30] can be used to calculate the eddy viscosity:

$$\nu_t = (C_s \Delta)^2 |\mathbf{S}| \tag{14}$$

where

$|\mathbf{S}| = (2S_{ij} S_{ij})^{0.5}$ and C_s is the Smagorinsky constant (0.1–0.2) [31]. In the simulation of this work, C_s was used as 0.12.

4 Viscosity and Turbulence Models

Some different proposals are presented in the literature to model the diffusive terms in the SPH approximation of the momentum conservation equation. The approaches to the diffusive terms (Ψ^a) used in this work are presented below.

4.1 Artificial viscosity (Π_{ab})

The artificial viscosity formulation [32, 33] is used in fluid flow simulation instead of the diffusive viscous terms in the momentum equation. It is commonly applied because of its simplicity. However, it is important to note that employed this way, the artificial viscosity becomes only a computational solution tool. For an adequate choice of some coefficients it is necessary to achieve the satisfactory simulation results. The form proposed in this article is shown in Eq. (15):

$$\Pi_{ab} = \begin{cases} \frac{-\alpha_\pi \mu^{ab} c^{ab}}{\rho^{ab}}, & \text{if } (\mathbf{v}^a - \mathbf{v}^b) \cdot (\mathbf{x}^a - \mathbf{x}^b) < 0, \\ 0, & \text{if } (\mathbf{v}^a - \mathbf{v}^b) \cdot (\mathbf{x}^a - \mathbf{x}^b) \geq 0. \end{cases} \tag{15}$$

$$\mu^{ab} = \frac{h^{ab} (\mathbf{v}^a - \mathbf{v}^b) \cdot (\mathbf{X}^a - \mathbf{X}^b)}{|\mathbf{X}^a - \mathbf{X}^b|^2 + \varphi^2}$$

$$c^{ab} = \frac{c^a + c^b}{2}, \rho^{ab} = \frac{\rho^a + \rho^b}{2}, h^{ab} = \frac{h^a + h^b}{2}.$$

The diffusive terms of the fixed particle modeled using the artificial viscosity is presented below.

$$\Psi^a = - \sum_{b=1}^n m^b \Pi_{ab} \nabla W(\mathbf{x}^a - \mathbf{x}^b, h) \tag{16}$$

Instabilities occur with the use of artificial viscosity. To reduce these undesirable effects arising from the use of this numerical correction, the use of conservative smoothing was proposed in the literature. However, the validated results were not presented for fluid flows in two or three dimensions [34–36].

4.2 Laminar shear stresses

The diffusive terms Ψ^a are the laminar shear stresses of the fixed particle, $(v^a \nabla^2 v^a)_{\text{LAMINAR}}$, which can be obtained from Eqs. (17) and (18), presented in [6] and [10], respectively:

$$\Psi^a = (v^a \nabla^2 v^a)_{\text{LAMINAR}} = \sum_{b=1}^n m^b \left[\frac{4v^a}{(\rho^a + \rho^b)} \frac{(\mathbf{x}^a - \mathbf{x}^b)}{|\mathbf{x}^a - \mathbf{x}^b|^2} \cdot \nabla W(\mathbf{x}^a - \mathbf{x}^b, h) \right] (\mathbf{v}^a - \mathbf{v}^b) \quad (17)$$

$$\Psi^a = (v^a \nabla^2 v^a)_{\text{LAMINAR}} = \sum_{b=1}^n m^b \left[\frac{2v^a}{\rho^b} \frac{(\mathbf{x}^a - \mathbf{x}^b)}{|\mathbf{x}^a - \mathbf{x}^b|^2} \cdot \nabla W(\mathbf{x}^a - \mathbf{x}^b, h) \right] (\mathbf{v}^a - \mathbf{v}^b) \quad (18)$$

The first proposal for laminar shear stresses—Eq. (17)—is used in the SPPhysics code [6] and the second one in the computer code presented in [9, 10] utilized in the simulation of the collapse of a water column.

4.3 Laminar shear stresses + sub-grid scale (SGS) turbulence model

In this model, the diffusive terms Ψ^a are composed of two parcels, related to laminar shear stresses (Eqs. (17)–(18)) and sub-grid scale (SGS) shear stresses, as shown in Eq. (19):

$$\Psi_a = (v^a \nabla^2 v^a)_{\text{LAMINAR}} + \sum_{b=1}^n m^b \left[\frac{\tau^{*a}}{(\rho^a)^2} + \frac{\tau^{*b}}{(\rho^b)^2} \right] \cdot \nabla W(\mathbf{x}^a - \mathbf{x}^b, h) \quad (19)$$

where τ^* is the sub-grid scale (SGS) shear stress tensor—defined in Eq. (7).

The last term on the right hand side of Eq. (19) is presented in [6, 13, 23, 26].

4.4 Laminar shear stresses + artificial viscosity

In this approach, proposed in [38], the term related to laminar shear stresses is implemented as well as the term related to the artificial viscosity as shown in Eq. (20):

$$\Psi^a = (v^a \nabla^2 v^a)_{\text{LAMINAR}} - \sum_{b=1}^n m^b \Pi_{ab} \nabla W(\mathbf{x}^a - \mathbf{x}^b, h) \quad (20)$$

The last term on the right-hand side of Eq. (20) is presented in Eq. (16) and works as a numerical correction to avoid numerical instabilities and the interpenetration among particles.

From the physical point of view, in problems involving mainly shock waves there is conversion of kinetic energy into heat. That energy transformation can be represented as a form of viscous dissipation and needs to be measured; which is carried out with the artificial viscosity. It should be noted that in [37] the objective of the authors when applying the artificial viscosity was different from that presented in subsect. 4.1 (in which the artificial viscosity directly replaced the viscous terms in the momentum equation).

This modeling was implemented by the authors of this paper. It was utilized, and the results analyzed, in the second

case studied (presented in Sect. 5.2: the collapse of a water column).

5 Numerical simulations

In this paper, simulations have been performed for the generation and propagation of waves on a flat beach and collapse of a water column, presented below.

5.1 Generation and propagation of waves on a flat beach

Three zones can be delimited in a beach: wave breaking zone, surf zone and swash zone. In the breaking zone the dissipation of the wave energy occurs. The surf zone is the region in which the wave propagates after the break. The swash zone, located immediately, is important because a substantial part of the total coastal sediment transport occurs in this region. On the coast line, the movement of the wave is forward, climbing the beach (run-up), and backward, descending the beach (run-down), delimiting the swash zone [38]. The action of breaking waves and run-up results in a highly complex movement, comprising medium and orbital movements and fluctuations (turbulence).

The Lagrangian simulations were performed with and without the use of a turbulence model.

5.1.1 Software

The computational tools employed in the wave simulations were the SPPhysics and FUNWAVE2D non-commercial software.

The first software is an open computer code developed in FORTRAN programming language and based on smoothed-particle hydrodynamics (SPH) for the study of free surface flows [6, 13]. It is the result of collaboration by researchers from Johns Hopkins University (USA), the University of Vigo (Spain) and the University of Manchester (UK). SPPhysics presents the options to use artificial viscosity, laminar shear stresses or laminar shear stress + SGS shear stresses (for turbulence modeling) in simulations.

FUNWAVE2D is a non-commercial FORTRAN software, produced by the Center for Applied Coastal Research (CACR, Delaware, USA). This code employs the numerical method of finite differences to solve the Boussinesq-type nonlinear wave equations and to simulate surface waves in coastal areas including internal and external surf zones. The wave breaking is treated using a formulation of artificial turbulent viscosity. A simple eddy viscosity-type formulation is used to calculate the wave energy dissipation caused by the wave breaking [39]. A validation study of this software (from laboratory data) applied to the simulation of wave

propagation in deep waters and shoaling zones up to the breaking region is in [40].

5.1.2 Simulated domain, initial and boundary conditions

It was simulated a beach domain with 2.75 m in extension in the inclined region (with an angle of 4.2364°). The amplitude and period of the wave were 0.01 m and 1.40 s, respectively, and the water level 0.18 m. The water was considered a viscous, incompressible and isothermal fluid. The kinematic viscosity was $1.0 \times 10^{-6} \text{ m}^2/\text{s}$.

In the SPHysics simulations, the Lagrangian SPH method was employed to solve the conservation equations of mass and momentum, Eqs. (1) and (2). Considering an isothermal flow of water, the energy conservation equation does not need to be solved. In the discretization of the domain, 4,221 water particles were employed from 0.00 to 3.75 m. The lateral distance between the centers of mass of two neighboring particles was 0.01 m. The support radius was defined as 0.013 m (approximately 1.30 times the initial spacing between the centers of mass of the particles). Dynamic boundary particles—described in [6]—were disposed on the contours (fixed bottom of the beach and paddle). An amount of 387 fixed particles was used to represent the bottom of the beach and 31 mobile particles were fixed initially at the position 0.13 m of the domain to represent the motion of the flap-type wavemaker. The search for neighboring particles was made using the linked list technique [41]. Two link lists were used in the search for neighboring particles. The first one tracked the boundary particles of the wavemaker and the second one tracked the fluid particles. The wave amplitude was 0.02 m. In the Tait equation, the coefficient B was $7.175 \times 10^5 \text{ kg/ms}^2$ and ρ^0 was $1,000 \text{ kg/m}^3$. Shepard filter was used in the density renormalization every 30 time steps. Kernel correction or kernel gradient correction [6] were not applied. A time step of $4.5 \times 10^{-5} \text{ s}$ was used to simulate the generation and propagation of the waves over a time simulation of 30.00 s. Figure 2 shows the geometry, the particles disposed inside the domain (in blue), on the paddle (mobile, in red) and on the bottom of the channel (immobile, in black).

In the Eulerian simulations carried out aiming to verify the SPH results, the FUNWAVE2D software was used. A domain mesh with 156 nodes in the horizontal direction and 21 nodes in the vertical direction was used. The spacing between dots in the horizontal direction was 0.05 m with a total horizontal distance of 7.75 m. Vertically, the spacing varied with the total depth, given by $H = h + \eta$, where h is the mean sea level and η is the surface elevation, defining a sigma-type mesh.

The dimensions of the Eulerian domain ranged from -4.00 to 3.75 m . The time simulated was 30.0 s, with a time increment of $1.0 \times 10^{-3} \text{ s}$ during the simulations. The wave breaking was treated by an artificial turbulent viscosity formulation, which can promote a more realistic description of the beginning and the end of the wave breaking in quantitative terms (in terms of the dissipated energy) [40, 42, 43]. For the time integration, in both Eulerian and Lagrangian simulations, the predictor–corrector method was used and the CFL number assumed a value of 0.20.

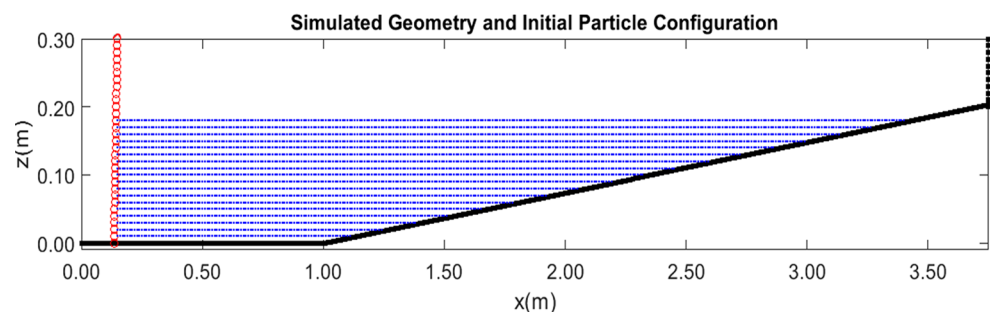
5.1.3 Results and discussion

SPH simulations were performed for three different treatments of the diffusive terms present in Eq. (2): (a) laminar shear stresses; (b) laminar shear stresses + SGS shear stresses; and (c) artificial viscosity, with $\alpha_\pi = 0.05, 0.20$ and 0.30 .

The wave period was 1.40 s and the wave amplitude was 0.01 m in all cases. The simulation results were plotted and the wave elevations can be shown in Figs. 3, 4, 5, 6. The reaching of the wave over the beach and its elevation are shown in the time instants 10.0, 15.0, 20.0 and 28.0 s, for different modelings of viscosity and turbulence.

The results are present in Tables 2, 3, 4, 5, 6, 7, 8, 9 and Figs. 3, 4, 5, 6. They can be divided into two groups. The first is composed by the results provided by the physical modelings for the diffusive terms, that is, laminar shear stresses and laminar shear stresses + SGS shear stresses (in the first two lines of Figs. 3, 4, 5, 6). The second group has as elements the SPH results achieved when

Fig. 2 Simulated geometry and initial setup of the fluid and boundary particles



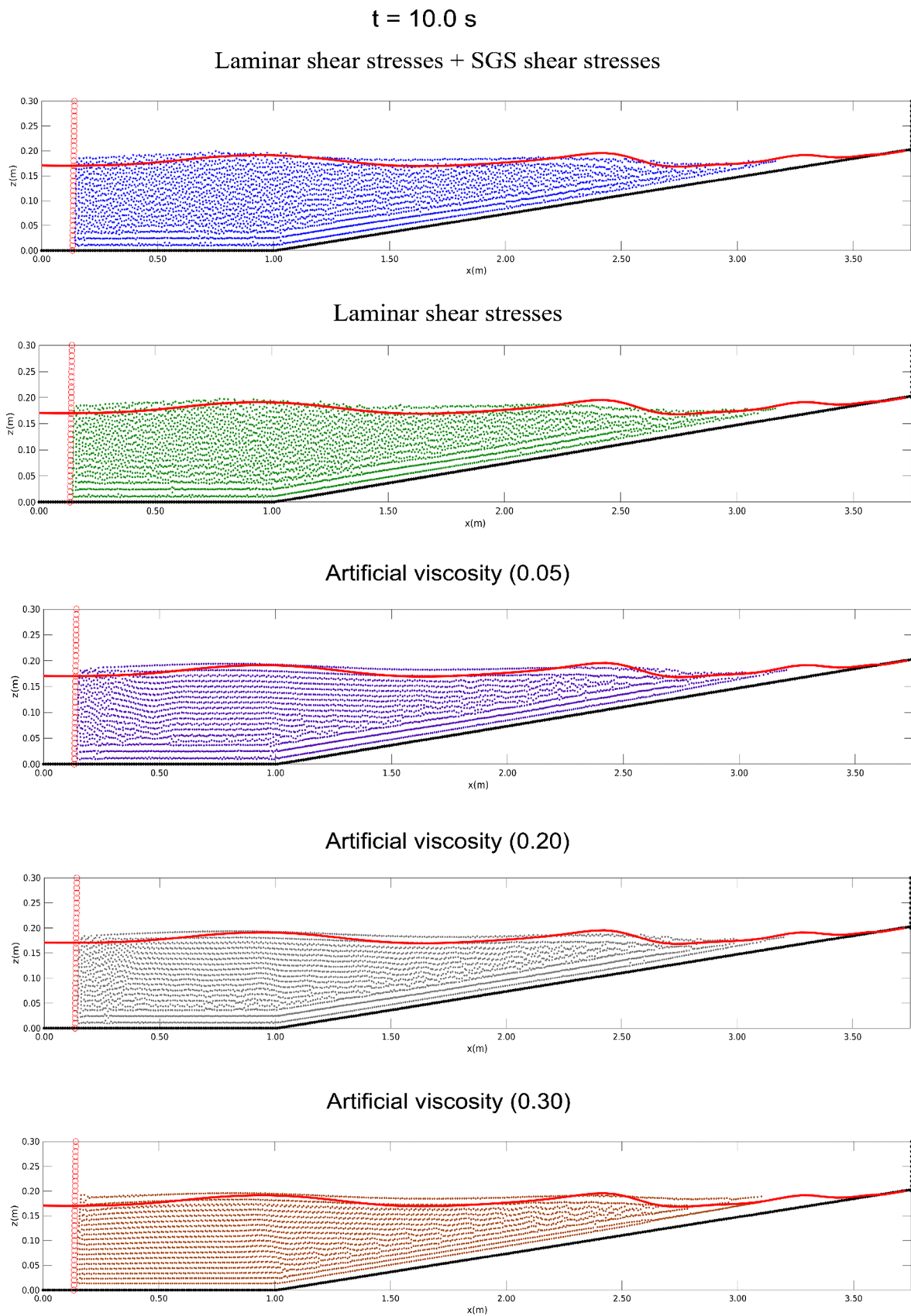


Fig. 3 SPH and Eulerian (red line) simulation results at $t = 10.0$ s. From the top of the page: laminar shear stresses + SGS shear stresses, laminar shear stresses and artificial viscosity modelings (with $\alpha_x = 0.05, 0.20$ and 0.30 , respectively)

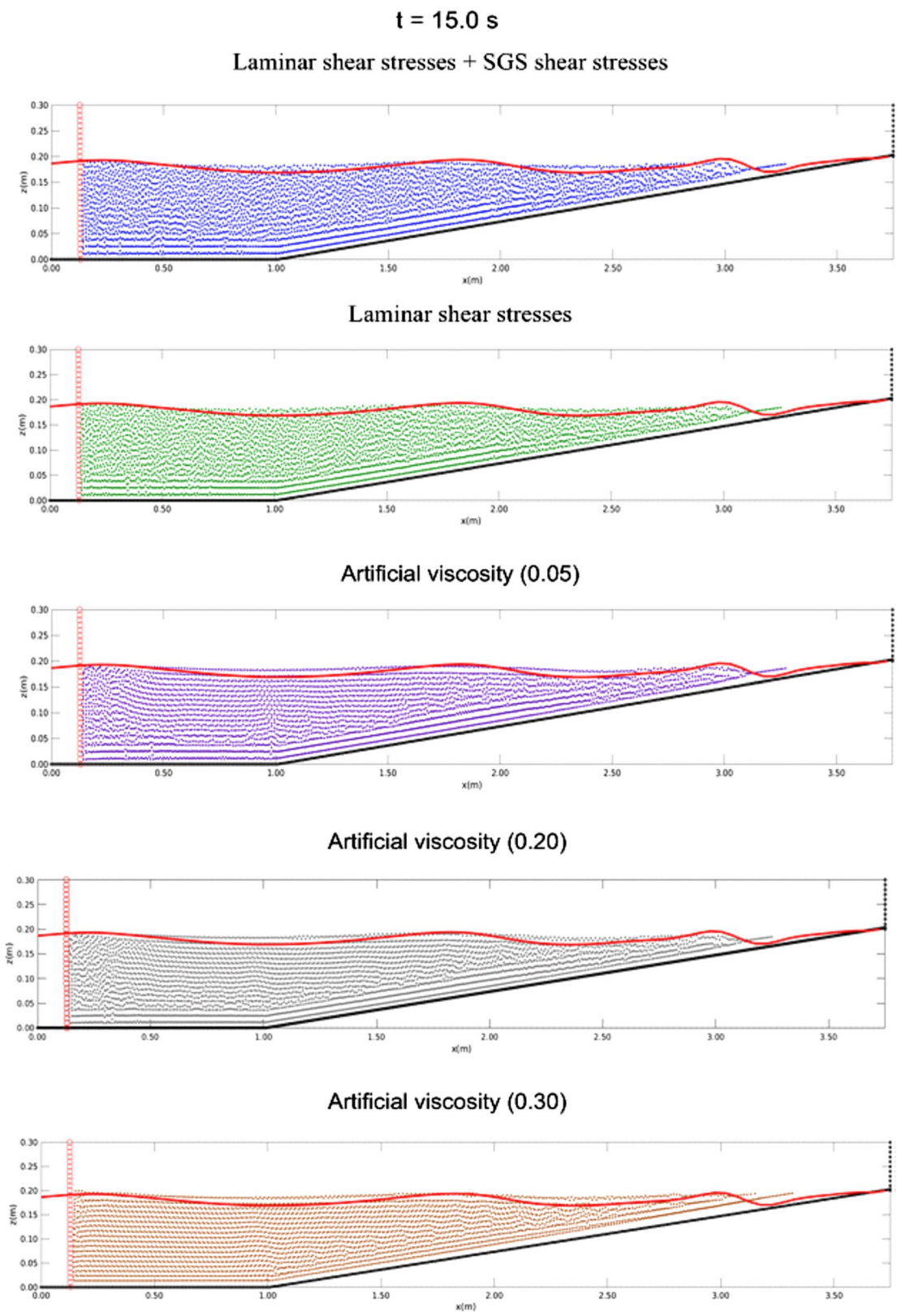


Fig. 4 SPH and Eulerian (red line) simulation results at $t=15.0$ s. From the top of the page: laminar shear stresses +SGS shear stresses, laminar shear stresses and artificial viscosity modelings (with $\alpha_x=0.05, 0.20$ and 0.30 , respectively)

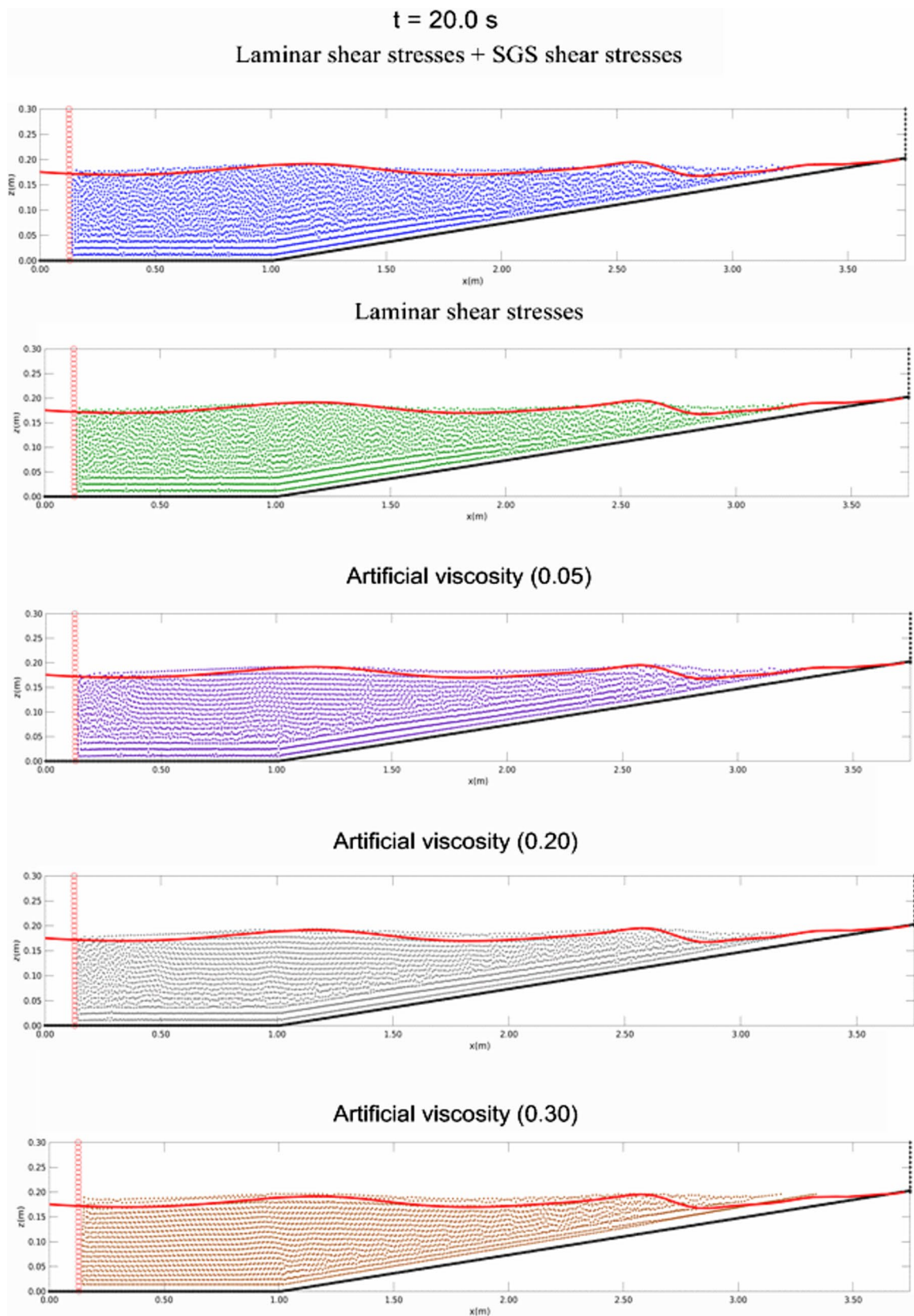


Fig. 5 SPH and Eulerian (red line) simulation results at $t=20.0 \text{ s}$. From the top of the page: laminar shear stresses + SGS shear stresses, laminar shear stresses and artificial viscosity modelings (with $\alpha_\pi=0.05, 0.20$ and 0.30 , respectively)

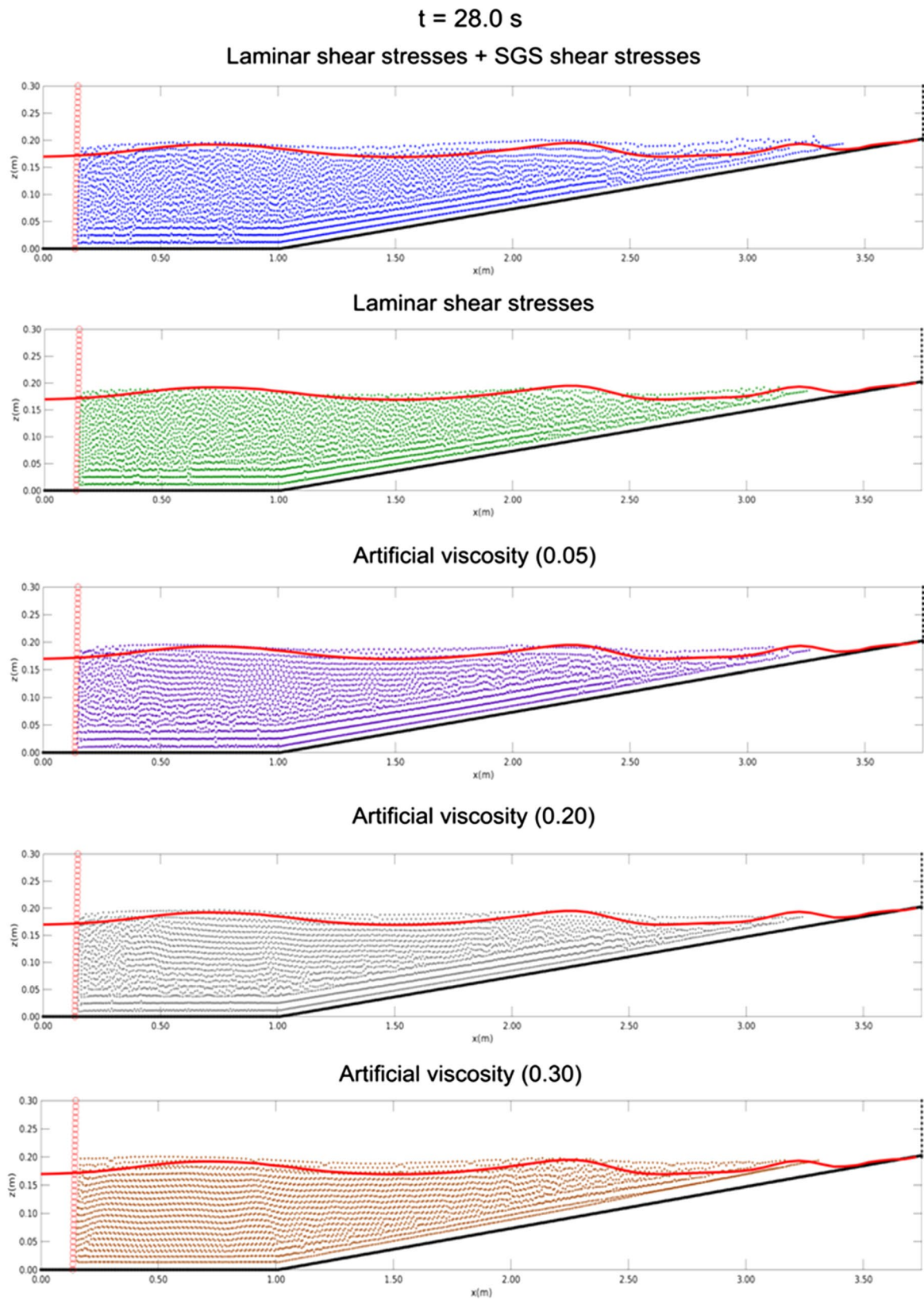


Fig. 6 SPH and Eulerian (red line) simulation results at $t=28.0$ s. From the top of the page: laminar shear stresses + SGS shear stresses, laminar shear stresses and artificial viscosity modelings (with $\alpha_\tau=0.05, 0.20$ and 0.30 , respectively)

the artificial viscosity was solely employed as a purely computational modeling to the diffusive terms present in Eq. (2)—in the third and fourth lines of Figs. 3, 4, 5, 6.

From the results presented in Table 2, the percentage relative errors between the modelings 2–6 and 1 (defined as standard) were calculated, as shown in Table 3. The last line in the table presents the average of the relative errors along the points in the domain where the free surface elevations were measured.

From the results presented in Table 4, the percentage relative errors between the modelings 2–6 and 1 (defined as standard) were calculated, as shown in Table 5. The last line in the table presents the average of the relative errors along the points in the domain where the free surface elevations were measured.

From the results presented in Table 6, the percentage relative errors between the modelings 2–6 and 1 (defined as standard) were calculated, as shown in Table 7. The last line in the table presents the average of the relative errors along the points in the domain where the free surface elevations were measured.

From the results presented in Table 8, the percentage relative errors between the modelings 2–6 and 1 (defined as standard) were calculated, as shown in Table 9. The last line in Table presents the average of the relative errors along the points in the domain where the free surface elevations were measured.

Analyzing the free surface elevation results, in the first group, it was verified that the laminar shear stresses modeling resulted in wave elevations more adjusted to those provided by the Eulerian modeling—the Boussinesq-type nonlinear wave equations, used as standard of comparison and presented in Appendix, mainly from $t=20.0$ s. However,

Table 3 Percentage relative error between the results achieved from the modelings 2–6 and Boussinesq-type nonlinear wave equations at $t = 10.0$ s

Position at the domain (m)	2 (%)	3 (%)	4 (%)	5 (%)	6 (%)
0.25	10.92	6.90	10.92	6.90	10.34
0.50	9.50	8.38	9.50	7.82	9.50
0.75	4.69	3.65	3.65	2.60	2.08
1.00	2.09	1.57	4.19	3.14	2.62
1.25	0.00	4.40	6.59	6.04	4.95
1.50	5.20	7.51	9.83	8.67	7.51
1.75	7.51	7.51	11.56	8.67	7.51
2.00	5.08	5.08	6.78	3.95	7.34
2.25	2.11	4.21	0.53	1.05	0.00
2.50	2.63	6.84	3.16	1.05	0.00
2.75	5.33	4.73	5.92	6.51	9.47
3.00	2.84	3.98	1.14	1.70	4.55
Average of the relative errors	4.89	4.91	6.26	5.00	6.14

the results obtained from the laminar shear stresses + SGS shear stresses approach showed, in general, a good agreement with the Eulerian modeling, according to the previous results shown in [44]. In particular, at $t=28.0$ s, higher differences in wave elevations were noted, when comparing this last modeling with the reference Eulerian results. In conclusion, in the physical modeling of the diffusive terms, the effects of the turbulence were not significant—due to the low Reynolds number in the period and wave amplitude simulated.

The second group of results (in last three lines of Figs. 3, 4, 5, 6 and modelings 4 to 6 in Tables 2, 3, 4, 5, 6, 7, 8, 9) showed that the application of the artificial viscosity in the

Table 2 Free surface elevation at $t = 10.0$ s (in meters)

Position at the domain (m)	Modeling applied					
	1*	2	3	4	5	6
0.25	0.174	0.193	0.186	0.193	0.186	0.192
0.50	0.179	0.196	0.194	0.196	0.193	0.196
0.75	0.192	0.201	0.199	0.199	0.197	0.196
1.00	0.191	0.187	0.194	0.199	0.197	0.196
1.25	0.182	0.182	0.190	0.194	0.193	0.191
1.50	0.173	0.182	0.186	0.190	0.188	0.186
1.75	0.173	0.186	0.186	0.193	0.188	0.186
2.00	0.177	0.186	0.186	0.189	0.184	0.190
2.25	0.190	0.186	0.182	0.189	0.188	0.190
2.50	0.190	0.185	0.177	0.184	0.188	0.190
2.75	0.169	0.178	0.177	0.179	0.180	0.185
3.00	0.176	0.171	0.169	0.178	0.179	0.184

*1-Boussinesq-type nonlinear wave equations; 2-Laminar + SGS Shear Stresses; 3-Laminar Shear Stresses; 4-Artificial Viscosity (with $\alpha_\pi=0.05$); 5-Artificial Viscosity (with $\alpha_\pi=0.20$); 6-Artificial Viscosity (with $\alpha_\pi=0.30$)

Table 4 Free surface elevation at $t = 15.0$ s (in meters)

Position at the domain (m)	Modeling applied					
	1*	2	3	4	5	6
0.25	0.197	0.193	0.191	0.189	0.189	0.197
0.50	0.189	0.184	0.182	0.189	0.190	0.187
0.75	0.176	0.188	0.186	0.189	0.185	0.187
1.00	0.171	0.183	0.181	0.184	0.185	0.187
1.25	0.175	0.183	0.185	0.189	0.185	0.187
1.50	0.184	0.191	0.194	0.193	0.190	0.191
1.75	0.197	0.191	0.189	0.189	0.190	0.190
2.00	0.189	0.178	0.180	0.189	0.190	0.186
2.25	0.171	0.182	0.180	0.188	0.185	0.180
2.50	0.176	0.181	0.180	0.184	0.185	0.185
2.75	0.184	0.185	0.188	0.184	0.185	0.189
3.00	0.197	0.189	0.188	0.193	0.180	0.185

*1-Boussinesq-type nonlinear wave equations; 2-Laminar + SGS Shear Stresses; 3-Laminar Shear Stresses; 4-Artificial Viscosity (with $\alpha_\pi=0.05$); 5-Artificial Viscosity (with $\alpha_\pi=0.20$); 6- Artificial Viscosity (with $\alpha_\pi=0.30$)

momentum equation can lead to the reasonable numerical results (depending on the best choice of the coefficient α_π , which is a function of the problem studied) although a purely computational term is applied in the substitution of the diffusive terms Ψ^α .

Regarding the maximum wave elevations (at the end of the wet region, on the sloping area of the beach), the Boussinesq-type nonlinear wave equations provided the highest values in the simulations (18.8, 19.0, 19.4 and 19.6 cm in the time instants 0.10, 0.15, 0.20 and 0.28 s, respectively). The

maximum differences between the wave elevations provided by the Eulerian and Lagrangian models were: +0.8 cm at $t = 10.0$ s (comparing 1st and 4th modelings), +0.5 cm at $t = 15.0$ s (comparing 1st and 5th modelings), +1.4 cm at $t = 20.0$ s (comparing 1st and 5th modelings) and +1.4 cm at $t = 28.0$ s (comparing 1st and 4th modelings).

Reference [33] is a study that presents an analysis of the effects of the artificial viscosity in simulations of propagation of regular waves.

5.2 Collapse of a water column

5.2.1 SPHysics simulations (using artificial viscosity, laminar shear stresses and laminar + SGS shear stresses)

SPHysics software has been used to simulate the collapse of the water column. Laboratory experiments shown in [11, 12] have been used in the validation of this computational tool for utilization in this case. The software has been used in simulations presented in this subsection.

5.2.1.1 Simulated domain, initial and boundary conditions The dimensions of the tank were $4.00\text{ m} \times 4.00\text{ m}$ and the water column had a width of 1.00 m and an initial height of 2.00 m. The particles were arranged with an initial separation between their centers of mass of 3.00 cm. The time step started at 1.00×10^{-4} s, varying, and it was calculated by the criterion presented in [6].

The continuity and momentum equations were solved. The Tait equation was used to predict the particle pressure field. The coefficient B was equal to $2.803 \times 10^5\text{ kg/ms}^2$ and

Table 5 Percentage relative error between the results achieved from the modelings 2–6 and Boussinesq-type nonlinear wave equations at $t = 15.0$ s

Position at the domain (m)	2 (%)	3 (%)	4 (%)	5 (%)	6 (%)
0.25	2.03	3.05	4.06	4.06	0.00
0.50	2.65	3.70	0.00	0.53	1.06
0.75	6.82	5.68	7.39	5.11	6.25
1.00	7.02	5.85	7.60	8.19	9.36
1.25	4.57	5.71	8.00	5.71	6.86
1.50	3.80	5.43	4.89	3.26	3.80
1.75	3.05	4.06	4.06	3.55	3.55
2.00	5.82	4.76	0.00	0.53	1.59
2.25	6.43	5.26	9.94	8.19	5.26
2.50	2.84	2.27	4.55	5.11	5.11
2.75	0.54	2.17	0.00	0.54	2.72
3.00	4.06	4.57	2.03	8.63	6.09
Average of the relative errors	3.93	4.67	4.30	4.59	4.46

Table 6 Free surface elevation at $t=20.0$ s (in meters)

Position at the domain (m)	Modeling applied					
	1*	2	3	4	5	6
0.25	0.175	0.179	0.177	0.177	0.183	0.186
0.50	0.175	0.184	0.182	0.186	0.187	0.191
0.75	0.184	0.188	0.186	0.191	0.192	0.195
1.00	0.191	0.185	0.191	0.191	0.191	0.200
1.25	0.191	0.188	0.191	0.191	0.191	0.200
1.50	0.179	0.188	0.182	0.191	0.191	0.195
1.75	0.175	0.184	0.178	0.186	0.186	0.191
2.00	0.175	0.184	0.182	0.186	0.186	0.191
2.25	0.184	0.188	0.182	0.186	0.190	0.191
2.50	0.197	0.193	0.191	0.191	0.194	0.195
2.75	0.179	0.188	0.182	0.195	0.189	0.195
3.00	0.179	0.184	0.182	0.186	0.184	0.195

*1-Boussinesq-type nonlinear wave equations; 2-Laminar + SGS Shear Stresses; 3-Laminar Shear Stresses; 4-Artificial Viscosity (with $\alpha_\pi=0.05$); 5-Artificial Viscosity (with $\alpha_\pi=0.20$); 6-Artificial Viscosity (with $\alpha_\pi=0.30$)

ρ^0 was $1,000 \text{ kg/m}^3$. The treatment of boundaries occurred through the dynamic contour particles. In order to avoid the tensile instability and the interpenetration between particles, SPHysics applied the artificial pressure proposed in [45]. The density correction was done with the Shepard filter every 30 time steps. Kernel correction or kernel gradient correction were not utilized. The XSPH method was used

for a more ordered movement of the particles during the simulation time. A description of these numerical corrections is in [6].

Table 7 Percentage relative error between the results achieved from the modelings 2–6 and Boussinesq-type nonlinear wave equations at $t = 20.0$ s

x(m)	2 (%)	3 (%)	4(%)	5 (%)	6 (%)
0.25	2.29	1.14	1.14	4.57	6.29
0.50	5.14	4.00	6.29	6.86	9.14
0.75	2.17	1.09	3.80	4.35	5.98
1.00	3.14	0.00	0.00	0.00	4.71
1.25	1.57	0.00	0.00	0.00	4.71
1.50	5.03	1.68	6.70	6.70	8.94
1.75	5.14	1.71	6.29	6.29	9.14
2.00	5.14	4.00	6.29	6.29	9.14
2.25	2.17	1.09	1.09	3.26	3.80
2.50	2.03	3.05	3.05	1.52	1.02
2.75	5.03	1.68	8.94	5.59	8.94
3.00	2.79	1.68	3.91	2.79	8.94
Average of the relative errors	2.97	1.68	3.86	4.46	7.61

5.2.1.2 Results and discussion Different modelings of viscosity and turbulence were applied in the simulations. Figure 7 shows the graphical results obtained using (a) artificial viscosity ($\alpha_\pi=0.10$), (b) laminar shear stresses and (c) laminar shear stresses + SGS shear stresses. The modeling (a), using artificial viscosity and $\alpha_\pi=0.10$, whose results were presented in [13], was taken as reference in the comparison of the results.

Differences were observed between the simulation results. The behavior of the waves has shown agreement at the time instant 0.38 s—the vertical line in Fig. 7 shows that the wave fronts presented abscissas near 2.20 m in all simulations.

In $t=0.86$ s, the heights of the waves over the tank wall were different: (a) 1.46 m; (b) 1.69 m and (c) 1.58 m. The separation among particles, after the impact against the tank wall, were observed. The final heights of 1.92 and 1.86 m were achieved by the detached particles in the simulations (b) and (c), respectively. In $t=1.30$ s, the detachment of particles was more visible in the modelings (b) and (c).

The model that employed the laminar shear stress treatment for the viscosity (c) presented a result with a reasonable agreement with the validated simulation (a)—which used the artificial viscosity, with $\alpha_\pi=0.10$. The waveforms

Table 8 Free surface elevation at $t=28.0$ s (in meters)

Position at the domain (m)	Modeling applied					
	1*	2	3	4	5	6
0.25	0.179	0.189	0.188	0.191	0.193	0.197
0.50	0.192	0.200	0.187	0.199	0.197	0.201
0.75	0.195	0.200	0.191	0.195	0.197	0.197
1.00	0.186	0.192	0.182	0.191	0.193	0.193
1.25	0.174	0.188	0.178	0.186	0.189	0.189
1.50	0.169	0.192	0.182	0.191	0.189	0.189
1.75	0.173	0.195	0.181	0.191	0.189	0.189
2.00	0.185	0.199	0.189	0.199	0.193	0.193
2.25	0.197	0.203	0.189	0.191	0.189	0.182
2.50	0.176	0.195	0.181	0.186	0.189	0.189
2.75	0.172	0.190	0.180	0.186	0.189	0.189
3.00	0.176	0.202	0.188	0.191	0.185	0.189

*1-Boussinesq-type nonlinear wave equations; 2-Laminar + SGS Shear Stresses; 3-Laminar Shear Stresses; 4-Artificial Viscosity (with $\alpha_\pi=0.05$); 5-Artificial Viscosity (with $\alpha_\pi=0.20$); 6-Artificial Viscosity (with $\alpha_\pi=0.30$)

Table 9 Percentage relative error between the results achieved from the modelings 2–6 and Boussinesq-type nonlinear wave equations at $t = 28.0$ s

Position at the domain (m)	2 (%)	3 (%)	4 (%)	5 (%)	6 (%)
0.25	5.59	5.03	6.70	7.82	10.06
0.50	4.17	2.60	3.65	2.60	4.69
0.75	2.56	2.05	0.00	1.03	1.03
1.00	3.23	2.15	2.69	3.76	3.76
1.25	8.05	2.30	6.90	8.62	8.62
1.50	13.61	7.69	13.02	11.83	11.83
1.75	12.72	4.62	10.40	9.25	9.25
2.00	7.57	2.16	7.57	4.32	4.32
2.25	3.05	4.06	3.05	4.06	7.61
2.50	10.80	2.84	5.68	7.39	7.39
2.75	10.47	4.65	8.14	9.88	9.88
3.00	14.77	6.82	8.52	5.11	7.39
Average of the relative errors	7.81	3.45	6.80	6.25	7.50

were qualitatively similar in all modelings applied during the simulated time.

5.2.2 (Laminar shear stresses + artificial viscosity) SPH Simulations

The literature [46] presented a model in which the viscous terms were modeled using laminar shear stresses + artificial viscosity, and RBC. When the artificial viscosity is applied in direct substitution of the diffusive terms of the

Navier–Stokes equations (often used in SPH simulations) it is a purely computational model for the fluid viscosity without physical meaning. According to the approach of this subsection, the physical viscosity is implemented in conjunction with the artificial viscosity (which in this case works as a numerical correction to avoid numerical instabilities and the interpenetration between particles). A complete presentation of the simulations performed is in [46]. The

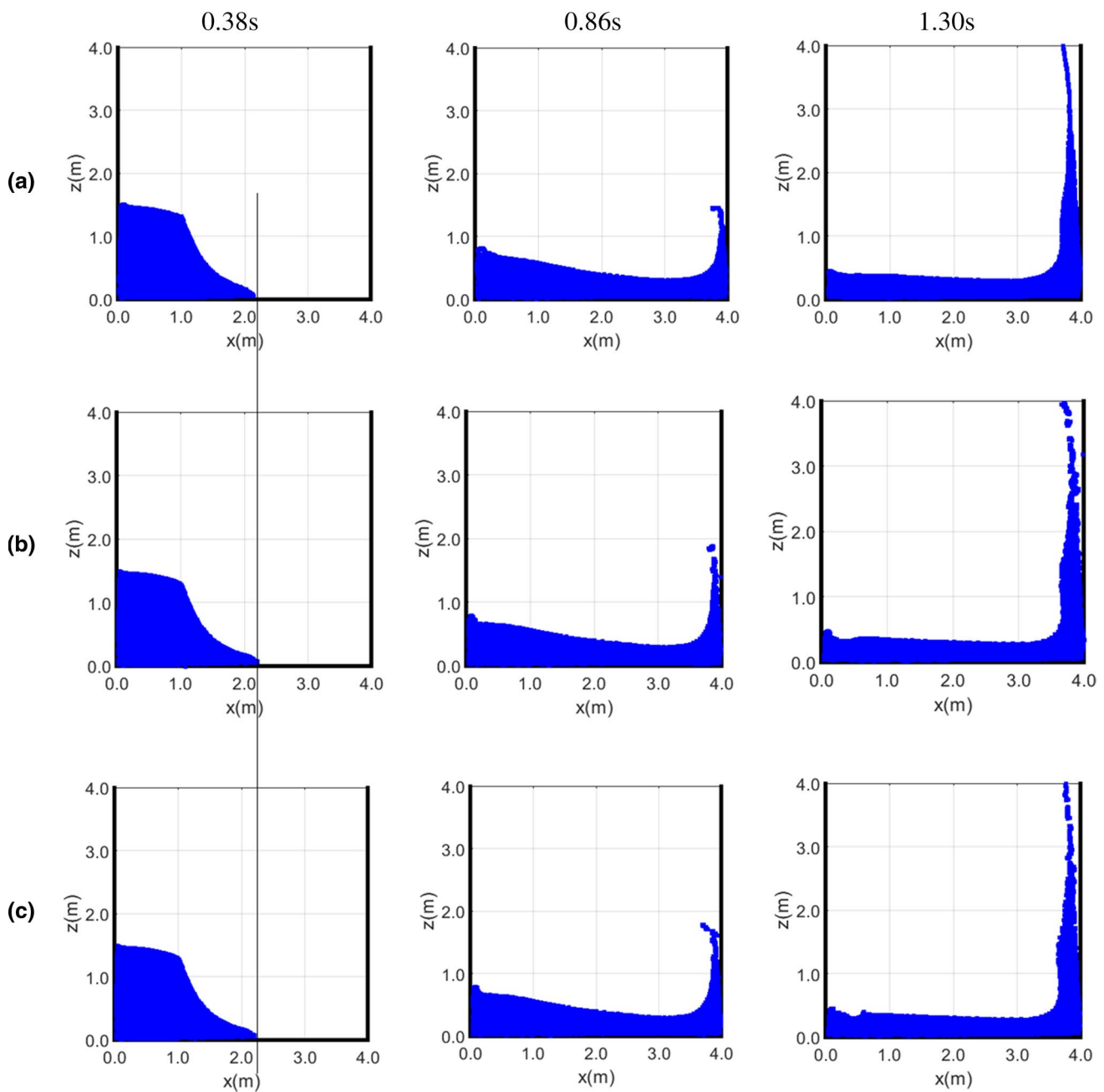


Fig. 7 SPH simulation results. **a** Artificial viscosity, with $\alpha_\pi=0.10$ (according to the results validated from laboratory data), presented in [13], **b** Laminar viscosity + SGS shear stresses modeling and **c** Laminar shear stresses modeling

computer code in which this approach was implemented is presented in [9, 10].

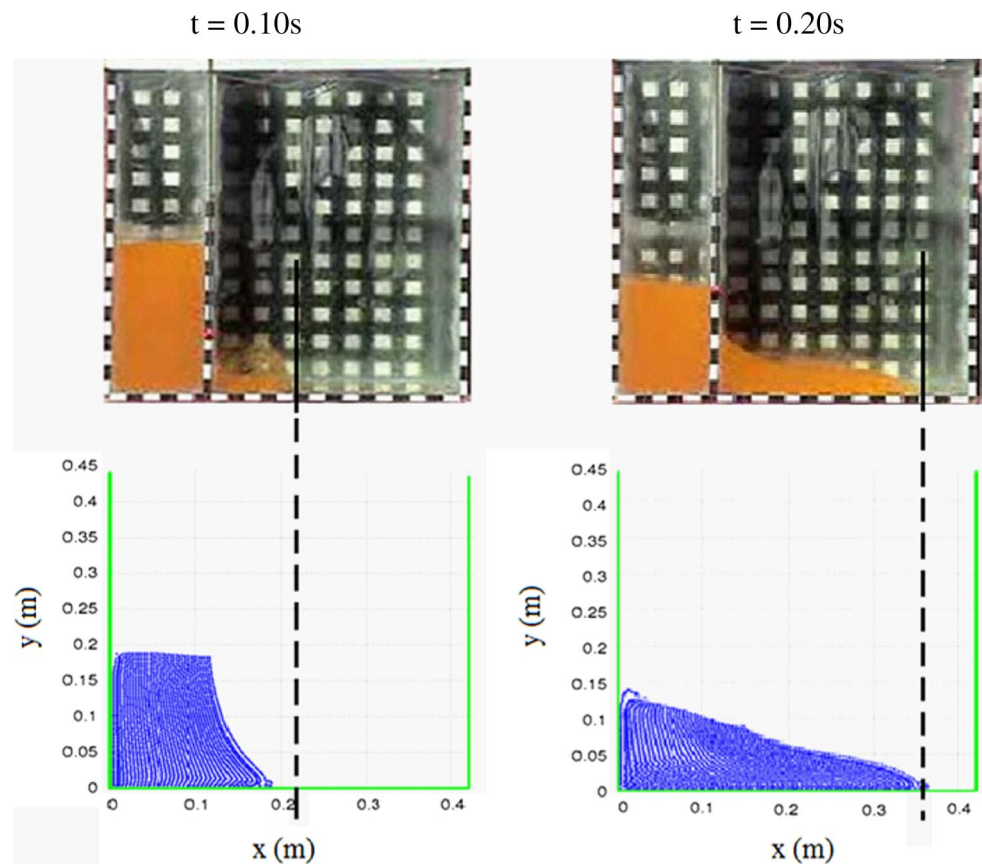
5.2.2.1 Results and discussion Figures 8 and 9 present the comparison of the positions of the wave fronts, based on the SPH simulations and experimental data provided by [47].

In the simulation using laminar shear stresses + artificial viscosity ($\alpha_\pi=0.20$), the differences between the numerical results and experimental data were 13.64% and 2.78% at

the time instants 0.10 and 0.20, respectively. When using laminar shear stresses + artificial viscosity ($\alpha_\pi=0.30$), those differences were 17.86% and 2.33%.

From the comparison between the numerical results and experimental data, it can be concluded that the formulation using laminar shear stresses + artificial viscosity and reflective boundary conditions [48] provides a consistent solution to the collapse of the wave column.

Fig. 8 Simulations employing (Laminar shear stresses + artificial viscosity, with $\alpha_\pi = 0.20$). At the first line, the experimental results are presented. The vertical dashed line is used to allow the comparison between the positions of the wave fronts



5.2.3 SPHysics (artificial viscosity) vs. (Laminar shear stresses + artificial viscosity) SPH simulations

The literature [37] presents a comparison between the simulations performed by SPHysics and the numerical code in which (laminar shear stresses + artificial viscosity) were implemented—described in [9, 10].

In that study, SPHysics used the artificial viscosity in substitution to the diffusive terms Ψ^a , dynamic particles were applied to the boundary treatment, and corrections of the pressure gradients near the contours were not carried out.

(Laminar shear stresses + artificial viscosity) modeling and reflective boundary conditions [48] were employed in the second computational simulation tool [9, 10]. A coefficient of restitution of kinetic energy equal to 1.00 (elastic collisions of the water particles against the tank walls) and density and pressure gradient corrections (CSPM) were employed in this numerical model.

5.2.3.1 Simulated domain, initial and boundary conditions The simulated geometry was a tank whose dimensions were 4.00×4.00 m. The water column had a width of 1.00 m and a height of 2.00 m.

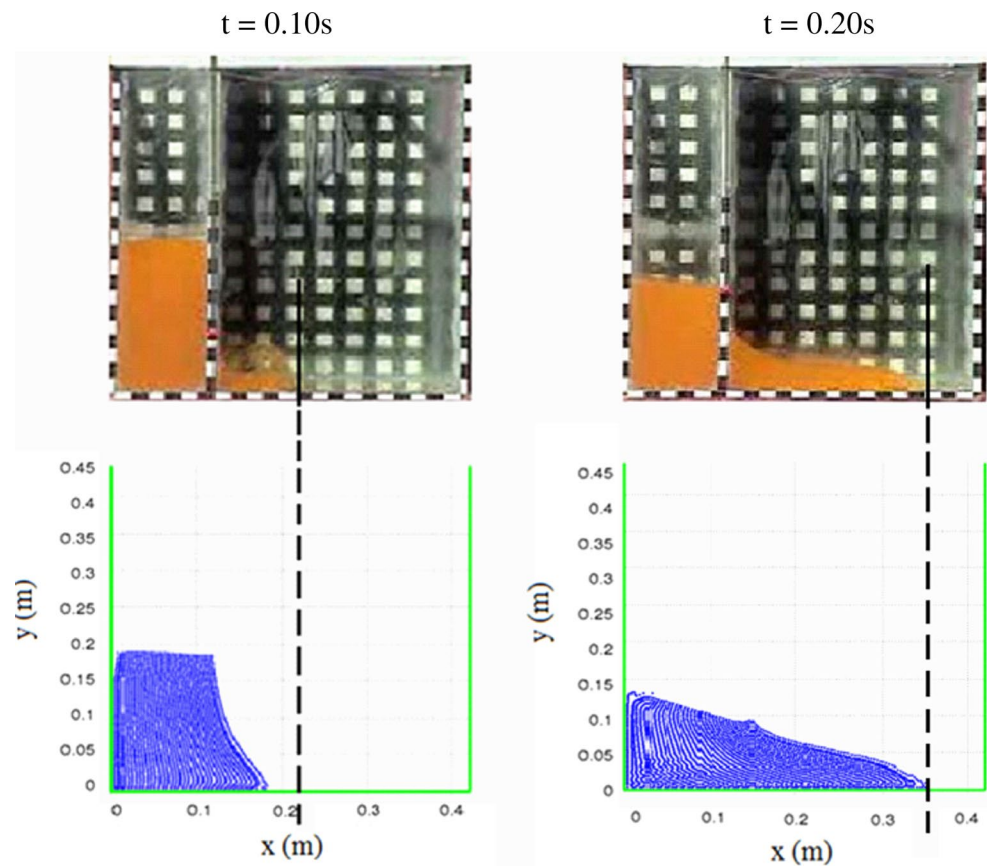
In the SPHysics, the particles were arranged with an initial separation between their centers of mass of 3.00 cm.

In the Tait equation, the coefficient B was 2.803×10^5 kg/ms² and ρ^0 was $1,000$ kg/m³. Shepard filter was used in the density correction every 30 time steps. Kernel correction and kernel gradient correction were not applied. Dynamic boundary particles were employed in the treatment of contours. The time step started at 1.00×10^{-4} s, varying, and it was calculated by the criterion presented in [6].

In the simulations performed using laminar shear stresses and artificial viscosity—in the code presented in [9, 10], the discretization of the fluid volume employed 2,556 particles with an initial lateral separation between the centers of mass of 2.86 cm. A cubic spline kernel was used in SPH interpolations. In the Tait equation, the coefficient B was 0.85×10^5 Pa and ρ^0 was $1,000$ kg/m³. The time step was 1.0×10^{-4} s (kept constant during the simulations). The coefficient of restitution of kinetic energy—in the implementation of the reflective boundary conditions [48]—was equal to 1.00. The density correction was applied by the Shepard filter every 30 time steps. The pressure gradients obtained by the SPH interpolations were corrected (using the CSPM method) at each numerical iteration.

Figure 10 presents, graphically, the simulation results at the time instants 0.40 s and 0.80 s. The simulations were performed employing $\alpha_\pi = 0.30$.

Fig. 9 Simulations employing (laminar shear stresses + artificial viscosity, with $\alpha_\pi = 0.30$). At the first line, the experimental results are presented. The vertical dashed line is used to allow the comparison between the positions of the wave fronts



From the results found, it is possible to verify an agreement between the positions of the wave fronts and wave heights in both simulations. Additionally, it is possible to state that it is possible to achieve the physical result through the employment of different modelings of Ψ^a , different boundary treatments and numerical corrections in the simulations. The results provided by the second modeling were physically consistent (using laminar shear stresses) and the numerical corrections (necessary due to the errors of the SPH method) were performed by the artificial viscosity implementation.

The achievement of the consistent results depends, therefore, on the adjustment of parameters in the simulations performed by different numerical codes.

6 Conclusions

This work presents an analysis of the modeling of the diffusive terms in the momentum equation of an incompressible and isothermal Newtonian fluid, according to the Lagrangian modeling and solution provided by the SPH method. Two cases were studied: propagation of waves on the beach and collapse of a water column.

In the first case study—which used SPHysics software in simulations, it was verified that the physical modeling of the diffusive viscous terms and turbulence, employing the laminar shear stresses, provided more adjusted wave elevations when compared to the Boussinesq-type nonlinear wave equations (Eulerian results provided by FUNWAVE code, whose validation is in [40]) in the wave period and wave amplitude simulated. However, the implementation of the artificial viscosity in the momentum equation led to the reasonable results for the wave elevations (due to the insignificance of the turbulence effects in the problem simulated), depending on the best choice of the coefficient α_π .

In the SPHysics simulations of the collapse of the water column (subsect. 5.2.1), the modeling that employed the laminar shear stresses presented results with reasonable agreement with the validated results of the literature with $\alpha_\pi = 0.10$ [13]. In the modeling using laminar + SGS shear stresses, the separation among particles was observed, from $t = 0.86$ s. The waveforms were similar in all modelings applied in the subsection in the simulated time.

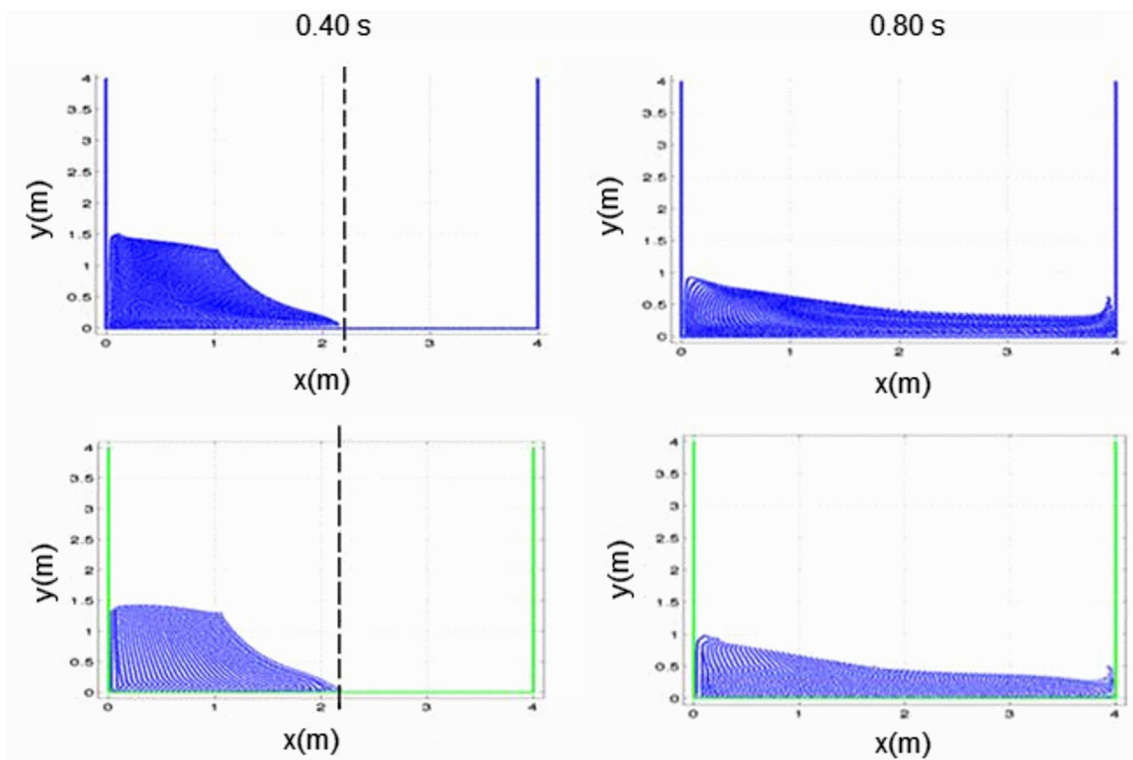


Fig. 10 At the top: graphical results of the SPHysics simulations—using artificial viscosity, $\alpha_\pi=0.30$. At the second line: the simulation results performed by the code presented in [9, 10], with laminar shear stresses + artificial viscosity ($\alpha_\pi=0.30$) Fraga Filho, CAD, Cha-

caltana, JTA. Revista Interdisciplinar de Pesquisa em Engenharia, 2(11), 2016; licensed under a Creative Commons Attribution (CC BY) license

In subsect. 5.2.3, the simulation results provided by the computer code, presented [9, 10], which was implemented using laminar shear stresses + artificial viscosity (with $\alpha_\pi = 0.30$) and reflective boundary conditions, and SPHysics simulations (using artificial viscosity treatment, with $\alpha_\pi = 0.30$, and dynamic boundary particles in the boundary treatment) were compared. Good agreement has been achieved between the results of the simulations. In the Tait equation, the coefficient B was 2.803×10^5 in SPHysics and equal to 0.85×10^5 Pa in the computer code implemented by the author, showing that is possible to reach good results through both computational tools, depending on the adjustment of different parameters in the diffusive models.

Appendix

Boussinesq-type nonlinear wave equations

These equations are obtained after integration of mass and momentum conservation equations in the vertical direction [49].

Continuity equation:

$$\frac{\partial \eta}{\partial t} + \frac{\partial M_i}{\partial x_i} = 0 \tag{A1}$$

where the flux M_i is:

$$M_i = (h + \delta\eta) \left\{ u_i + \chi^2 \left[\frac{1}{2} z^2 - \frac{1}{6} (h^2 - h\delta\eta + \delta^2 \eta^2) \right] \frac{\partial}{\partial x_i} \left(\frac{\partial u_j}{\partial x_j} \right) \right\} + \chi^2 \left[z + \frac{1}{2} (h - \delta\eta) \right] \frac{\partial}{\partial x_i} \left[\frac{\partial (hu_j)}{\partial x_j} \right] + O(\chi^4) \tag{A2}$$

Momentum equation:

$$\frac{\partial u_i}{\partial t} + \delta \left(u_j \frac{\partial u_i}{\partial x_j} \right) + \frac{\partial \eta}{\partial x_i} + \chi^2 J_i + \delta \chi^2 K_i = O(\chi^4) \quad (\text{A3})$$

where the nonlinear terms J_i and K_i are given as

$$J_i = \frac{1}{2} z^2 \frac{\partial}{\partial x_i} \left[\frac{\partial}{\partial x_j} \left(\frac{\partial u_j}{\partial t} \right) \right] + z \frac{\partial}{\partial x_i} \left[\frac{\partial}{\partial x_j} \left(h \frac{\partial u_j}{\partial t} \right) \right] - \frac{\partial}{\partial x_i} \left[\frac{1}{2} (\delta \eta)^2 \frac{\partial}{\partial x_j} \left(\frac{\partial u_j}{\partial t} \right) + \delta \eta \frac{\partial}{\partial x_j} \left(h \frac{\partial u_j}{\partial t} \right) \right] \quad (\text{A4})$$

$$K_i = \frac{\partial}{\partial x_i} \left\{ (z - \delta \eta) \left(u_j \frac{\partial}{\partial x_j} \right) \left[\frac{\partial (h u_j)}{\partial x_j} \right] + \frac{1}{2} (z^2 - \delta^2 \eta^2) \left(u_j \frac{\partial}{\partial x_j} \right) \left(\frac{\partial u_j}{\partial x_j} \right) \right\} + \frac{1}{2} \frac{\partial}{\partial x_i} \left\{ \left[\frac{\partial (h u_j)}{\partial x_j} + \delta \eta \frac{\partial u_j}{\partial x_j} \right]^2 \right\} \quad (\text{A5})$$

where the level z is the reference depth for calculating the velocities, which may be given as

$$z \approx 0.531 h_0 \quad (\text{A6})$$

where:

η is the free surface elevation.

h is the total water depth.

t is the time.

$\delta = a_0/h_0$ and $\chi = k_0 h_0$ are scales of nonlinearity and dispersion, respectively.

a_0, h_0, k_0 are, in sequence, the typical wave amplitude, the depth of water at rest and the number of waves.

$u_i = (u, v)$ is the velocity at depth in the coordinated z : $u_i = \left(\frac{\partial \phi}{\partial x_i} \right)$, ϕ being the velocity potential.

Acknowledgements The authors would like to thank ESS Engineering Software Steyr GmbH, Austria, for the support provided in carrying out simulations in this work. We would also like to thank SPHERIC—SPH rEsearch and engineeRing International Community and the developers of the SPHysics software for keeping it available for academic use.

A sincere thank you to Ana Carolina Vargas do Vale Amaro for her diligent English proofreading of this paper.

Funding This work was funded by the Federal Institute of Education, Science and Technology of Espírito Santo, Brazil, during Professor Fraga Filho's post-doctoral internship at ESS Engineering Software Steyr GmbH, Austria.

Availability of data and material The data and material that supports the findings of this study are available within the article.

Declaration

Conflict of interest The authors certify that they have no affiliations with or involvement in any organization or entity with any financial interest or non-financial interest in the subject matter or materials discussed in this manuscript.

References

- Biscarini C, Di Francesco S, Manciola P (2010) CFD modeling approach for dam break flow studies. *Hydrol Earth Syst Sci* 14:705–718. <https://doi.org/10.5194/hess-14-705-2010>
- Zheng X, Ma Q, Shao S (2018) Study on SPH Viscosity Term Formulations. *Appl Sci* 8(2):249. <https://doi.org/10.3390/app8020249>
- Molteni D, Colagrossi A (2009) A simple procedure to improve the pressure evaluation in hydrodynamic context using the SPH. *Comput Phys Commun* 180(6):861–872. <https://doi.org/10.1016/j.cpc.2008.12.004>
- Antuono M, Colagrossi A, Marrone S (2012) Numerical diffusive terms in weakly-compressible SPH schemes. *Comput Phys Commun* 183(12):2570–2580. <https://doi.org/10.1016/j.cpc.2012.07.006>
- Green MD, Vacondio R, Peiró J (2019) A smoothed particle hydrodynamics numerical scheme with a consistent diffusion term for the continuity equation. *Comput Fluids* 179:632–644. <https://doi.org/10.1016/j.compfluid.2018.11.020>
- Gesteira MG, Rogers BD, Dalrymple RA, Crespo AJC, Narayanaswamy M (2010) User Guide for SPHysics Code. University of Manchester, UK. Available at https://wiki.manchester.ac.uk/sphysics/images/SPHysics_v2.2.000_GUIDE.pdf, accessed on 15 July, 2020.
- Kirby JT, Lon W, Shi F (2005) FUNWAVE 2.0: Fully Nonlinear Boussinesq Wave Model on Curvilinear Coordinates. Part I. Model Formulations. Delaware, US: University of Delaware, Center for Applied Coastal Research, Dept of Civil & Environmental Engineering.
- Kirby JT, Lon W, Shi F (2005) FUNWAVE 2.0: Fully Nonlinear Boussinesq Wave Model on Curvilinear Coordinates. Part II. User's Manual. Delaware, US: Center for Applied Coastal Research, Department of Civil and Environmental Engineering, 2005.
- Fraga Filho CAD (2016) Development of a Computer Code using the Lagrangian Smoothed Particle Hydrodynamics (SPH) Method for Solution of Problems in Fluid Dynamics and Heat Transfer. In: Proceedings of the XXXVII Ibero-Latin American Congress of Computational Method in Engineering—CILAMCE 2016, November 6–9, Brasília, DF, Brazil. Available at <http://periodicos.unb.br/index.php/ripe/article/view/14444/12755>, accessed on 15 July, 2021.
- Fraga CAD (2017) Development of a computational instrument using a lagrangian particle method for physics teaching in the areas of fluid dynamics and transport phenomena. *Rev Bras Ensino Fís* 39(4):e4401. <https://doi.org/10.1590/1806-9126-rbef-2016-0289>
- Crespo AC, Dominguez JM, Barreiro A, Gómez-Gesteira M, Rogers BD (2006) GPUs, a new tool of acceleration in CFD: efficiency and reliability on Smoothed Particle Hydrodynamics methods. *PLoS ONE* 6(6):e20685. <https://doi.org/10.1371/journal.pone.0020685>
- Kleefsman KMT, Fekken G, Veldman AEP, Iwanowski B, Buchner B (2005) A Volume-of-Fluid based simulation method for wave impact problems. *J Comput Phys* 206:363–393. <https://doi.org/10.1016/j.jcp.2004.12.007>

13. Gomez-Gesteira M, Rogers BD, Crespo AJC, Dalrymple RA, Narayanaswamy M, Dominguez JM (2012) SPHysics-development of a free surface fluid solver-Part 1: Theory and formulations. *Comput Geosci* 48:289–299. <https://doi.org/10.1016/j.cageo.2012.02.029>
14. Fraga CAD (2019) Smoothed particle hydrodynamics fundamentals and basic applications in continuum mechanics. Springer Nature, Switzerland
15. Robinson M, Monaghan JJ (2012) Direct numerical simulation of decaying two-dimensional turbulence in a no-slip square box using smoothed particle hydrodynamics. *Inte J Numer Methods Fluids* 70:37–55. <https://doi.org/10.1002/flid.2677>
16. Violeau D, Issa R (2007) Numerical modelling of complex turbulent free-surface flows with the SPH method: an overview. *Inte J Numer Methods Fluids* 53:277–304. <https://doi.org/10.1002/flid.1292>
17. Menzies K (2009) Large eddy simulation applications in gas turbines. *Phil Trans R Soc A* 367(2827–2838):2009. <https://doi.org/10.1098/rsta.2009.0064>
18. Porte-Agel F, Meneveau C, Parlangé MB (2000) A scale-dependent dynamic model for large-eddy simulation: application to a neutral atmospheric boundary layer. *J Fluid Mech* 415:261–284. <https://doi.org/10.1017/S0022112000008776>
19. Bossuyt J, Meneveau C, Meyers J (2018) Large Eddy Simulation of a wind tunnel wind farm experiment with one hundred static turbine models. *J Phys: Conf Series* 1037(6):062006. <https://doi.org/10.1088/1742-6596/1037/6/062006>
20. Piomelli U (1999) Large-eddy simulation: achievements and challenges. *Prog Aerosp Sci* 35:335–362. [https://doi.org/10.1016/S0376-0421\(98\)00014-1](https://doi.org/10.1016/S0376-0421(98)00014-1)
21. Zhiyin Y (2015) Large-eddy simulation: Past, present and the future. *Chin J Aeronaut* 28(1):11–24. <https://doi.org/10.1016/j.cja.2014.12.007>
22. Mayrhofer A, Laurence D, Rogers BD, Violeau D (2015) DNS and LES of 3-D wall-bounded turbulence using smoothed particle hydrodynamics. *Comput Fluids* 115:86–97. <https://doi.org/10.1016/j.compfluid.2015.03.029>
23. Lo EYM, Shao S (2002) Simulation of Near-Shore Solitary Wave Mechanics by an Incompressible SPH Method. *Appl Ocean Res* 24(5):275–286. [https://doi.org/10.1016/S0141-1187\(03\)00002-6](https://doi.org/10.1016/S0141-1187(03)00002-6)
24. Shao SD, Gotoh H (2004) Simulating coupled motion of progressive wave and floating curtain-wall by SPH-LES model. *Coast Eng J* 46(2):171–202. <https://doi.org/10.1142/S0578563404001026>
25. Shao S, Ji C (2006) SPH computation of plunging waves using a 2-D sub-particle scale (SPS) turbulence model. *Int J Numer Methods Fluids* 51:913–936. <https://doi.org/10.1002/flid.1165>
26. Dalrymple RA, Rogers BD (2006) Numerical modeling of water waves with the SPH method. *Coast Eng* 53:141–147. <https://doi.org/10.1016/j.coastaleng.2005.10.004>
27. Kirkil G, Mirocha J (2012) Implementation and evaluation of dynamic subfilter-scale stress models for Large-Eddy simulation using WRF*. *Mon Weather Rev* 140:266–284. <https://doi.org/10.1175/MWR-D-11-00037.1>
28. Su M, Chen Q, Chiang C-M (2001) Comparison of different subgrid-scale models of large eddy simulation for indoor airflow modelling. *J Fluids Eng* 123:628–639. <https://doi.org/10.1115/1.1378294>
29. Chow FK, Street RL (2009) Evaluation of turbulence closure models for Large-Eddy simulation over complex terrain: flow over Askervein Hill. *J Appl Meteorol Climatol* 48:1050–1065. <https://doi.org/10.1175/2008JAMC1862.1>
30. Smagorinsky J (1963) General circulation experiments with the primitive equations. I. The basic experiment. *Mon Wea Rev* 91(3):99–164. [https://doi.org/10.1175/1520-0493\(1963\)091%3c0099:GCEWTP%3e2.3.CO;2](https://doi.org/10.1175/1520-0493(1963)091%3c0099:GCEWTP%3e2.3.CO;2)
31. Gabreil E, Tait SJ, Shao S, Nichols A (2018) SPHysics simulation of laboratory shallow free surface turbulent flows over a rough bed. *J Hydraul Res* 56(5):727–747
32. Monaghan JJ (1992) Smoothed particle hydrodynamics. *Annual Rev Astron Appl* 30:543–574. <https://doi.org/10.1146/annurev.aa.30.090192.002551>
33. De Padova D, Dalrymple R, Mossa M (2014) Analysis of the artificial viscosity in the smoothed particle hydrodynamics modelling of regular waves. *J Hydraul Res* 52(6):836–848. <https://doi.org/10.1080/00221686.2014.932853>
34. Guenter C, Hicks DL, Swegle JW (1994) Conservative Smoothing versus Artificial Viscosity. Sandia Report SAND-94–1853, UC-705 <https://doi.org/10.2172/10187573>
35. Hicks DL, Liebrock LM (2004) Conservative smoothing with B-splines stabilizes SPH material dynamics in both tension and compression. *Appl Math Comput* 150(1):213–234. [https://doi.org/10.1016/S0096-3003\(03\)00222-4](https://doi.org/10.1016/S0096-3003(03)00222-4)
36. Frontiere N, Raskin CD, Owen JM (2017) CRKSPH—A conservative reproducing kernel smoothed particle hydrodynamics scheme. *J Comput Phys* 332:160–209. <https://doi.org/10.1016/j.jcp.2016.12.004>
37. Fraga Filho CAD, Chacaltana JTA (2016) Boundary Treatment Techniques in Smoothed Particle Hydrodynamics: Implementations in Fluid and Thermal Sciences and Results Analysis. In: Proceedings of the XXXVII Ibero-Latin American Congress of Computational Method in Engineering—CILAMCE 2016, Brasília, DF, Brazil. *Revista Interdisciplinar de Pesquisa em Engenharia*, 2(11). Available at <https://periodicos.unb.br/index.php/ripe/article/view/21270>, accessed on June 25, 2020.
38. Peregrini DH (1998) Surf zone currents. *Theoret Comput Fluid Dynamics* 10(1–4):295–309. <https://doi.org/10.1007/s001620050065>
39. Kennedy AB, Chen Q, Kirby JT, Dalrymple RA (2000) Boussinesq modeling of wave transformation, breaking, and runup I: 1D. *J Waterw, Port, Coastal, Ocean Eng* 126(1):39–47. [https://doi.org/10.1061/\(ASCE\)0733-950X\(2000\)126:1\(39\)](https://doi.org/10.1061/(ASCE)0733-950X(2000)126:1(39))
40. Bruno D, De Serio F, Mossa M (2009) The FUNWAVE model application and its validation using laboratory data. *Coast Eng* 56(7):773–787. <https://doi.org/10.1016/j.coastaleng.2009.02.001>
41. Fraga Filho CAD, Schuina LL, Porto BS (2020) An investigation into neighbouring search techniques in meshfree particle methods: an evaluation of the neighbour lists and the direct search. *Arch Computat Methods Eng* 27:1093–1107. <https://doi.org/10.1007/s11831-019-09345-9>
42. Chen Q, Kirby JT, Dalrymple RA, Kennedy AB, Chawla A (2000) Boussinesq modeling of wave transformation, breaking, and runup. II: 2D. *J Waterw, Port, Coastal, Ocean Eng* 126(1):39–47. [https://doi.org/10.1061/\(ASCE\)0733-950X\(2000\)126:1\(48\)](https://doi.org/10.1061/(ASCE)0733-950X(2000)126:1(48))
43. Chen Q, Kirby JT, Dalrymple RA, Wei F, Thornton EB (2003) Boussinesq Modeling of Longshore Currents. *Journal of Geophysical Research*, 108 (C11). <https://doi.org/10.1029/2002JC001308>
44. Fraga Filho CAD, Piccoli FP, Barbosa DA, Chacaltana JTA (2015) Numerical Study of the Propagation of Waves on Flat Beaches: An Application in Engineering using SPHysics and FUNWAVE Models. In: Proceedings of the 23rd ABCM International Congress of Mechanical Engineering, December 6–11, Rio de Janeiro, RJ, Brazil. <https://doi.org/10.20906/CPS/COB-2015-0561>
45. Monaghan JJ (2000) SPH without tensile instability. *J Comput Phys* 159(2):290–311. <https://doi.org/10.1006/jcph.2000.6439>
46. Fraga Filho CAD, Chacaltana JTA (2015) Study of Fluid Flows using Smoothed Particle Hydrodynamics: the modified Pressure Concept Applied to Quiescent Fluid and Dam Breaking. In: Proceedings of the XXXVI Ibero-Latin American Congress of Computational Method in Engineering—CILAMCE 2015, November 22–25, Rio de Janeiro, Brazil. <https://doi.org/10.20906/CPS/CILAMCE2015-0071>

47. Cruchaga MA, Celentano DJ, Tezduyar TE (2007) Collapse of a liquid column: numerical simulation and experimental validation. *Comput Mech* 39(4):453–476. <https://doi.org/10.1007/s00466-006-0043-z>
48. Fraga CAD (2017) An algorithmic implementation of physical reflective boundary conditions in particle methods: Collision detection and response. *Phys Fluids* 29:113602. <https://doi.org/10.1063/1.4997054>
49. Wei G, Kirby JT, Grilli ST, Subramanya R (1995) A fully nonlinear boussinesq model equations for surface waves. Part 1. highly nonlinear, unsteady waves. *J Fluid Mech* 294:71–92. <https://doi.org/10.1017/S0022112095002813>

Publisher's Note Springer Nature remains neutral with regard to jurisdictional claims in published maps and institutional affiliations.